Stability and evolution of the crystal structure of $TbBaCo_2O_{6-\delta}$ during thermal oxygen release/uptake

Ulises Amador[1], Rafael Marín[2], Clemens Ritter[3], Oscar Fabelo[3], M. Teresa Azcondo[1] and Susana García-Martín*,[2]

[1] Universidad San Pablo-CEU, CEU Universities, Facultad de Farmacia, Departamento de Química y Bioquímica, Urbanización Montepríncipe, Boadilla del Monte, E-28668, Madrid, Spain

[2] Departamento de Química Inorgánica I, Facultad de Ciencias Químicas, Universidad Complutense, 28040 Madrid, Spain

[3] Institut Laue-Langevin, 71 rue des Martyrs, CS20156, 38042 Grenoble Cedex 9, France

ABSTRACT: A-site ordered double perovskites with the general formula $LnBaCo_2O_{6-\delta}$ (where Ln is a lanthanide element) present electrical and electro-catalytic properties that makes them attractive as possible ceramic electrode-materials for solid oxide cells or alkaline electrolyzers. The properties are highly influenced by the anion vacancies concentration, which is strongly related to the Co-oxidation state, and their location in the structure. Awareness of the stable phases is essential to synthesize, evaluate and optimize the properties of $LnBaCo_2O_{6-\delta}$ oxides at operating conditions in different applications. $TbBaCo_2O_{6-\delta}$ are representative oxides of these layered perovskites systems. The present article reports a study of $TbBaCo_2O_{6-\delta}$ by electron diffraction, high resolution electron microscopy and powder neutron diffraction experiments at different temperatures. Synthesis of $TbBaCo_2O_{6-\delta}$ in air and slowly cooled to room temperature (RT) at 5 ºC h^{-1}, leads to samples formed by distinct phases with different oxygen contents and crystal structure. The 122 and 112 phases (with $a_p \times 2a_p \times 2a_p$ and $a_p \times a_p \times 2a_p$ unit cells respectively; a_p being the lattice parameter of the simple cubic perovskite structure) are predominant in quasi-equilibrium prepared samples (cooled at RT at 1 ºC h^{-1}) or prepared in Ar-flow and quenched to RT. The evolution of the crystal structure of $TbBaCo_2O_{6-\delta}$ during thermal oxygen release/uptaking consists of modulation from the 122-phase to the 112-phase (or vice versa during uptaking) by creation/occupation of anion vacancies within the $TbO_{1-\delta}$ planes. Anion vacancies are not detected in oxygen crystallographic position different that those located within the $TbO_{1-\delta}$ planes even at the highest temperatures, supporting the 2D character of the high anion conduction of the $LnBaCo_2O_{6-\delta}$ oxides.

1. INTRODUCTION

A-site ordered double perovskites with the general formula $LnBaCo_2O_{6-\delta}$ (where Ln is a lanthanide element) have been recognized as potential air electrodes for intermediate temperature solid oxide fuel cells (IT-SOFCs).[1-4] Besides, the catalytic activity for the hydrogen evolution reaction (HER)[5-7] and for the oxygen evolution reaction (OER)[8], recently reported in compounds of these systems, makes them as well attractive as possible ceramic electrode-materials for electrolyzers. The electrical and electro-catalytic properties of these oxides are intimately related to their crystal structure, in particular to the location of the anion vacancies within the oxygen sublattice.[9,10]

$GdBaCo_2O_{6-\delta}$ is one of the most studied compounds of such systems due to its low polarization resistance when used as electrode in symmetrical half cells.[11-13] The first study of the crystal structure of a sample of $GdBaCo_2O_{6-\delta}$ ($\delta \sim 0.6$) prepared in air concluded that it adopts a superstructure of the perovskite with orthorhombic unit cell $a_p \times 2a_p \times 2a_p$ (a_p being the lattice parameter of the simple cubic perovskite structure).[14] This so-called orthorhombic 122-type structure corresponds to the $GdBaCo_2O_{5.5}$ stoichiometry and pre-

sents layered-type ordering of the Gd and Ba atoms and additional ordering of the anion vacancies within the $GdO_{1-\delta}$ planes, giving rise to the corresponding ordering of the $CoO6$ octahedra and $CoO5$ pyramids (Figure 1a). This study also reported that when the $GdBaCo_2O_{6-\delta}$ was synthesized in Ar flow, the high content of anion vacancies ($\delta \sim 1$) leads to oxygen-empty Gd-planes and to a tetragonal $a_p \times a_p \times 2a_p$ unit cell constituted by $CoO5$ pyramids (the tetragonal 112-type structure) (Figure 1b).[14] Further studies assigned either the orthorhombic 122-type or the 112-type crystal structure to $LnBaCo_2O_{6-\delta}$ oxides depending on δ values lower or higher than 0.5 respectively[15-19] and described a reversible phase transition from the 122-type to the tetragonal 112-type accompanied by oxygen loss when the oxides are thermally treated.[20,21] In addition to these two oxygen-content dependent perovskite-superstructures, a superstructure with a $3a_p \times 3a_p \times 2a_p$ unit cell has been reported for $GdBaCo_2O_{6-\delta}$ single crystals with $\delta \sim 0.62$ [22] and a $4a_p \times 4a_p \times a_p$ supercell in $TbBaCo_2O_{4.5}$ obtained by topotactic reduction of $TbBaCo_2O_{5.5}$.[23] More recently, a study of $EuBaCo2O_{5.5}$ reports a $2a_p \times 2a_p \times 2c_p$ supercell that combines the Eu and Ba ordering along c with the ordering of Co^{3+}

square pyramids and octahedra alternating along b and orbital-order alternating along a. The orbital ordering is lost at 365 K leading to the $a_p \times 2a_p \times 2a_p$ supercell.[24] Contrasting insights into the crystal structure and electrical properties of different $GdBaCo_2O_{6-\delta}$ phases obtained under different synthesis conditions have been reported.[13] This last work stated that $GdBaCo_2O_{6-\delta}$ with $\delta < 0.5$ was obtained when the oxide was prepared by the ceramic method in air and relatively slow cooling (5 °C/h); however, $\delta > 0.5$ values were achieved when synthesized under Ar flow. Most importantly, the study revealed that single phase $GdBaCo_2O_{6-\delta}$ was only obtained when the oxide was prepared in Ar. SAED and HRTEM results showed the co-existence of two different phases in the sample synthesized in air and slowly cooled: one with a $\sqrt{2}a_p \times \sqrt{2}a_p \times 2a_p$ unit cell and another one with a $a_p \times a_p \times 2a_p$ cell. These two phases, which according to the XEDS analysis presented the same Gd/Ba stoichiometric atomic ratio, must differ in the anion sublattice in such a way that the $\sqrt{2}a_p \times \sqrt{2}a_p \times 2a_p$ cell accommodates higher oxygen contents. On the contrary, the $GdBaCo_2O_{6-\delta}$ with $\delta > 0.5$, which was prepared in Ar, presented the tetragonal 112-type structure. In the course of this work, a metastable phase with $a_p \times 3a_p \times 2a_p$ unit cell was detected in a $GdBaCo_2O_{6-\delta}$ sample with average value of $\delta{\sim}0.67$, which was prepared in air and rapidly cooled, showing that the rate of cooling in air is also a relevant parameter. It is noteworthy that similar thermal influence on the phase stability and crystal structure was reported by C. Frontera *et al.* for the system $PrBaCo_2O_{6-\delta}$.[25]

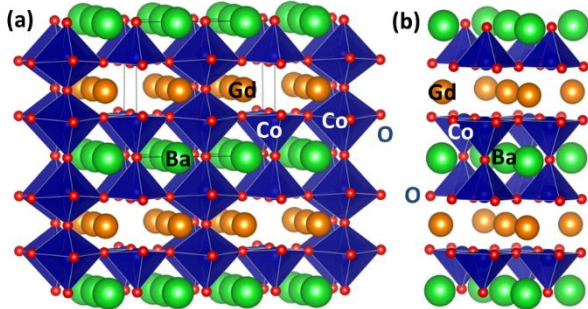**Figure 1**. Schematic representation of the structure of the $GdBaCo_2O_{6-\delta}$ phases; (a) 122-like and (b) 112-like.

Resuming one can state that the $LnBaCo_2O_{6-\delta}$ systems show a wide range of oxygen non-stoichiometry modulated within different perovskite-type structures that emerge from the location of the oxygen vacancies within the $LnO_{1-\delta}$ planes. The synthesis conditions highly affect the formation of different phases of the compounds, which present different oxygen contents and crystal structures and hence, different properties. Therefore, awareness of the stable phases is essential to synthesize, evaluate and optimize the properties of $LnBaCo_2O_{6-\delta}$ oxides at operating conditions in different applications. In this context, knowing the structure of $LnBaCo_2O_{6-\delta}$ oxides at high temperature in air, as well as its evolution from room temperature, is relevant for their application as air-electrode components in SOFCs. We present in here a new study of the crystal structure of $TbBaCo_2O_{6-\delta}$ synthesized under different conditions by means of selected

area electron diffraction (SAED), high resolution transmission electron microscopy (HRTEM) and neutron powder diffraction (NPD) at different temperatures. $TbBaCo_2O_{6-\delta}$ is isostructural with $LnBaCo_2O_{6-\delta}$ (Ln = Gd, Pr). We confirm the extreme sensibility of the phase formation to the synthesis conditions and show the structural evolution occurring by oxygen-vacancy accommodation during thermal treatments.

2. EXPERIMENTAL

Considering previous results on $GdBaCo_2O_{6-\delta}$[13] and with the aim of obtaining different oxygen contents, we have prepared $TbBaCo_2O_{6-\delta}$ by solid state method in air and different cooling approaches. The samples have been prepared by using Tb_2O_3 (Sigma Aldrich, 99.99%), $BaCO_3$ (Sigma Aldrich, 99.99%) and Co_2O_3 (Sigma Aldrich, 99.99%). Tb_2O_3 was heated at 900 °C prior to weighing. Stoichiometric amounts of the starting compounds were ground together and heated at 1000 °C for 12 h for decarbonation in air. Afterwards, the samples were again ground, pelleted and then fired at 1200 °C in air. Finally, the samples in powder form were submitted to different cooling treatments after heating at 1200 °C in air another 12 h. One of the samples was quenched from that temperature to room temperature (RT), a second sample was cooled to RT at 5 °C h^{-1} and the third one was cooled to RT in quasi-equilibrium conditions at 1 °C h^{-1}. According to these cooling conditions, the samples are called in the text Q-TBCO, 5C-TBCO, and 1C-TBCO.

Crystalline phase identification and sample purity were assessed from X-ray powder diffraction (XRPD) data collected on a Bruker D8 high-resolution $\theta/2\theta$ diffractometer in Bragg-Bentano geometry equipped with a LynxEye® fast detector using monochromatic $CuK\alpha_1$ ($\lambda = 1.5406$ Å) (radiation obtained with a germanium primary monochromator). Diffraction data were analyzed using the Fullprof software.[26] XRPD patterns were mostly used for phase identification by La Bail method[27] since detailed structural analyses were performed using NPD as described below.

Selected area electron diffraction (SAED) and high-resolution transmission electron microscopy (HRTEM) studies have been performed with a JEOL JEM 3000F microscope operating at 300 kV (double tilt ($\pm$ 20º) (point resolution 1.7Å)), fitted with an XEDS microanalysis system (OXFORD INCA). The atomic ratio of the metals has been determined by X-ray energy dispersive spectroscopy (XEDS) analyses finding good agreement between analytical and nominal composition in all the crystals. For transmission electron microscopy the samples were ground in n-butyl alcohol and ultrasonically dispersed. A few drops of the resulting suspension were deposited in a carbon-coated grid.

Neutron powder diffraction (NPD) was used to study the samples, either at RT or by thermo-diffraction up to 900 ºC. The sample Q-TBCO was measured at 102ºC (in its paramagnetic domain, i.e., at a temperature sufficiently high avoid to any magnetic order to simplify the structural study). This pattern was recorded on the high-resolution diffractometer D2B (ILL, Grenoble); a monochromatic beam of wavelength 1.594 Å was selected with a Ge monochromator from the primary beam. The instrumental resolution was increased by reducing the divergence of the primary

beam by an additional 10' collimator. The instrumental contribution to the line broadening was determined using a NIST standard sample of $Na_2Ca_3Al_2F_{14}$, whereas a standard sample of Si (also from NIST) was used for precise determination of the wavelength.

NPD patterns as a function of temperature were collected for the 1C-TBCO sample from 200 °C to 800 °C in air (in a quartz tube open to air) on heating and cooling stages, on the D1B instrument at ILL, using a monochromatic beam of 1.28 Å. The contribution of the instrument to the peak width was determined by the instrument resolution function determined from a $Na_2Ca_3Al_2F_{14}$ standard sample, whereas the wavelength was determined using a Si standard. The temperature was changed at a rate of 10 °C/min and the sample was stabilized at every temperature for 30 minutes prior to recording the corresponding pattern.

Structural refinements using NPD data were performed by the Rietveld method using the FullProf software.[26] The neutron scattering amplitudes used in the refinements were 0.7380, 0.5070, 0.2490 and 0.5803 (10^{-12} cm) for Tb^{+3}, Ba^{+2}, Co^{+3}, and O^{2-}, respectively; isotropic thermal factors were employed for all atoms. Throughout the refinements, the perovskite A (Ba and Tb) and B (Co) sites were constrained to be fully occupied, but the chemical composition was refined, and a single thermal factor for all oxygen atoms was assumed.

3. RESULTS AND DISCUSSION

3.1. Sample prepared in air and cooled to room temperature at 5 °C h-1 (5C-TBCO).

Figure S1 shows the XRPD pattern of the 5C-TBCO sample. The pattern seems to correspond to a single orthorhombic 122-type phase, as suggested by the peaks indicated by arrows in Fig. S1: two reflections around 2θ angles 46.4° and 46.9° corresponding to d-spacings 1.94 Å and 1.96 Å, and the two weak reflections at 11.31° and 11.76°, corresponding to d-spacings 7.82 Å and 7.52 Å.

Figures 2, 3 and **4** show SAED patterns and HRTEM images of different crystals of the 5C-TBCO sample. The results indicate that the sample contains three different types of crystals (A, B and C). The patterns have been indexed according to the basic perovskite structure (p refers to simple cubic perovskite). All the SAED patterns show extra reflections at $G_p\pm1/2(001)_p$ characteristic of the layered-type ordering of Gd and Ba. In the A-type crystals, these $G_p\pm1/2(001)_p$ reflections appear along both $[001]_p$ and $[100]_p$ directions (Fig. 2a), which could be associated with doubling of two main a_p-parameters. However, Fig. 2c and d, that show the HRTEM images of two areas of a A-type crystal oriented along the $[010]_p$ zone axis and the corresponding fast Fourier transforms (FFTs), discard the doubling of two lattice parameters. Fig. 2c shows contrast differences characteristic of $a_p \times 2a_p$ periodicity and Fig. 2d shows two perpendicularly oriented domains with contrast differences indicating $a_p \times 2a_p$ periodicity in each of them. The FFT in Fig. 2c corresponds to only one domain and therefore shows the $G_p\pm1/2(001)_p$ reflections only along $[001]_p$. However, the FFT in Fig. 2d corresponds to the combination of both domains, like the SAED pattern in Fig. 2a. Therefore, the SAED

and HRTEM results in Fig. 2 conclude that the A-type crystals have a crystal structure with $a_p \times a_p \times 2a_p$ unit cell, characteristic of the 112-phase and present domains with perpendicular orientation of the structure.
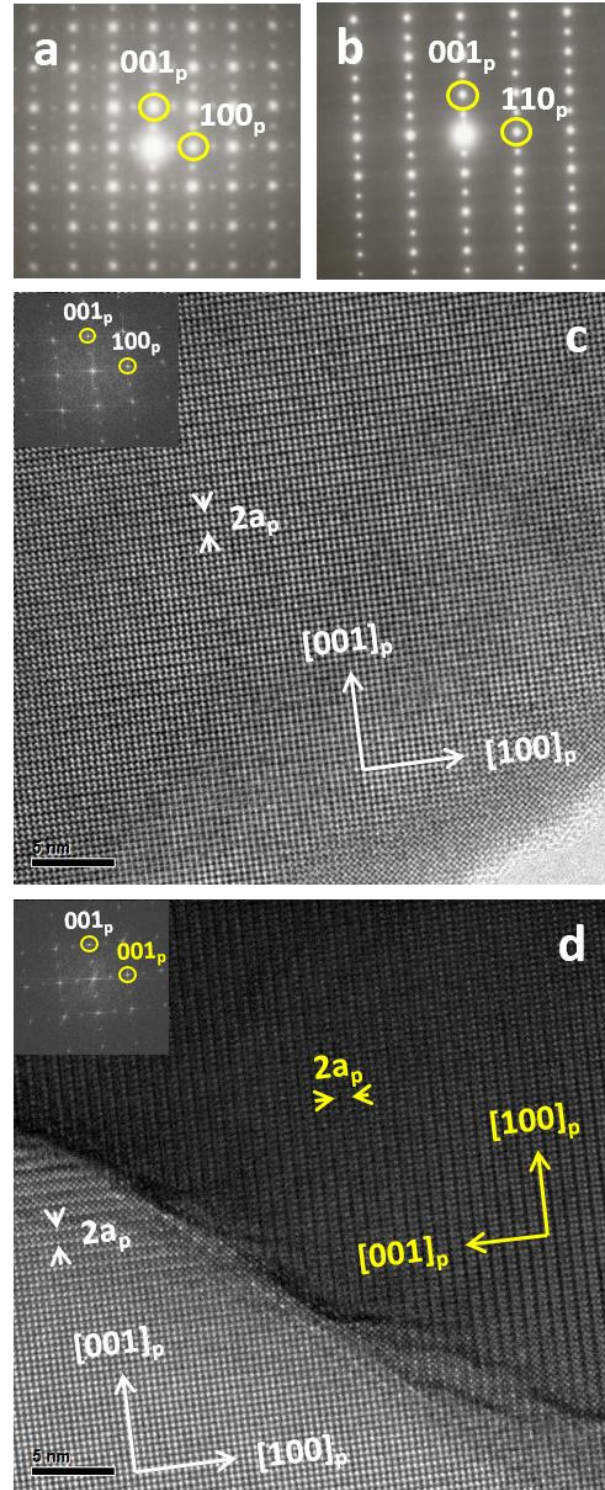

Figure 2. SAED patterns of an A-type crystal of 5C-TBCO along the a) $[010]_p$ and b) $[-110]_p$ zone axis; c) and d) HRTEM images and corresponding FFT of two areas of a A-type crystal along the $[010]_p$ zone axis.

The SAED patterns of the B-type crystals in Fig. 3a and b show extra reflections at $Gp\pm1/2(110)_p$ in addition to the

Gp±1/2(001)$_p$ reflections (also along two perpendicular directions like the A-type crystals). The presence of the Gp±1/2(110)$_p$ reflections is characteristic of a 2a$_p$ × 2a$_p$ × 2a$_p$ unit cell, or a$_p$ × 2a$_p$ × 2a$_p$ or √2a$_p$ × √2a$_p$ × 2a$_p$ unit cells with domains of the cell oriented in perpendicular directions. Fig. 3c and d show HRTEM images oriented along the [010]$_p$ zone axis. The images again reveal two perpendicularly oriented domains with contrast differences indicating a$_p$ × 2a$_p$ periodicity characteristic of √2a$_p$ × √2a$_p$ × 2a$_p$ unit cell. Interestingly, in the crossing areas between two domains with a$_p$ × 2a$_p$ periodicity, there are domains showing contrast differences with 2a$_p$ × 2a$_p$ periodicity of the a$_p$ × 2a$_p$ × 2a$_p$ unit cell characteristic of the 122-phase. Fig. 3c shows a crystal with bigger domains of 2a$_p$ × 2a$_p$ periodicity than those of the crystal in Fig. 3d.
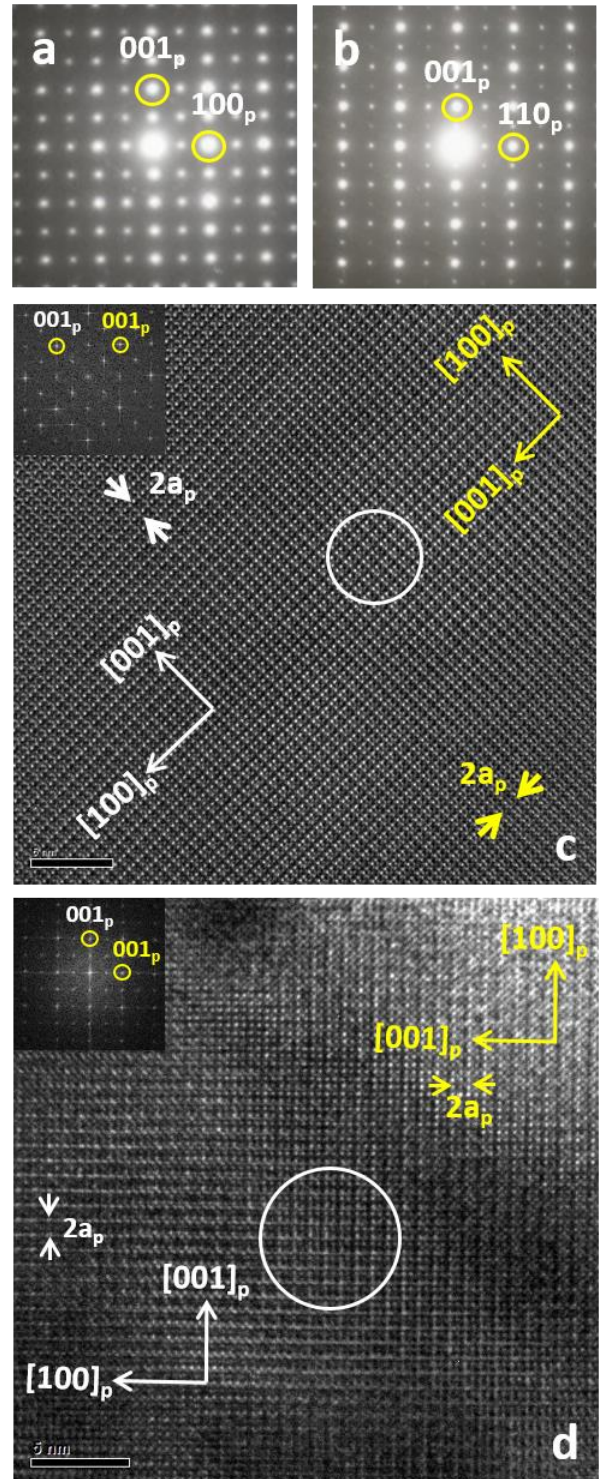

Figure 3. SAED patterns of a B-type crystal of 5C-TBCO along the a) [010]$_p$ and b) [-110]$_p$ zone axis; c) and d) HRTEM images and corresponding FFT of two B-type crystals along the [010]$_p$ zone axis.

Figure 4 displays a characteristic SAED pattern along the [100]$_p$ zone axis (Fig. 4a) and the corresponding HRTEM (Fig. 4b) of the C-type crystals. The patterns shows extra reflections at G$_p$±1/3(010)$_p$ and the image clearly reveals domains with contrast differences with 3a$_p$ × 2a$_p$ periodicity characteristic of the

$a_p \times 3a_p \times 2a_p$ unit cell. The pattern also shows weak extra reflections at $G_p \pm 1/2(010)_p$ associated to the 122-phase domains and even weaker reflections at $G_p \pm 1/6(010)_p$ probably due to double diffraction.
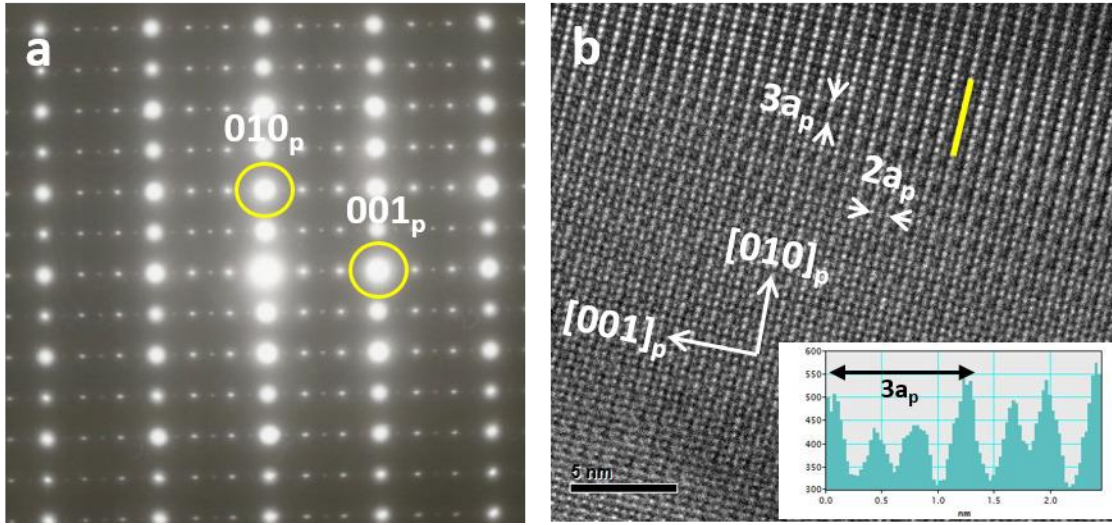
This 132 superstructure, also associated to ordering of oxygen-vacancies, was detected for the first time in $GdBaCo_2O_{6-\delta}$.[13]

Figure 4. a) SAED pattern of a C-type crystal of 5C-TBCO along the $[100]_p$ zone axis and b) corresponding HRTEM image. Notice that the cell orientation (123-like) is chosen to agree with that used for the fitting of the XRPD pattern (Fig.S1)

In conclusion, the SAED and HRTEM results of the 5C-TBCO sample reveal that it consists of different phases of oxides with layered-type perovskite structure and probably with differences on the oxygen-content, since the EDX analysis indicate similar nominal atomic ratio of the metals in all types of crystals. One of the phases (found in type A crystals) corresponds to the 112-crystal structure with $a_p \times a_p \times 2a_p$ unit cell; the B-type crystals show two phases distributed in domains: one with $\sqrt{2}a_p \times \sqrt{2}a_p \times 2a_p$ unit cell ($\sqrt{2}\sqrt{2}2$-phase) and the 122-phase with $a_p \times 2a_p \times 2a_p$ unit cell. Type C crystals contain the 123-phase with $a_p \times 3a_p \times 2a_p$ unit cell. The uptake and accommodation of oxygen of the $TbBaCo_2O_{6-\delta}$ while cooling from high temperatures seems not to be uniform and originates crystals with domains having different oxygen contents leading to different layered-perovskite structures.

After the TEM results, we have proceeded to fit the XRPD data of the sample 5C-TBCO to either a single 122-phase or a phase mixture. Figure S1 depicts the best LeBail fitting. The sample contains three phases: 122-like, 112-like and the 132-like. Phases 122 and 112 are undoubtedly identified, the third phase seems to be present but in a very small amount; the strongest support of its existence is the presence of the very weak (040) reflection. The results agree with the TEM observations except that the $\sqrt{2}\sqrt{2}2$-phase is not detected by XRPD, probably due to the small size of the domains that contain this phase and the extremely weak reflections associated to the tilting of the oxygen-octahedra of

the CoO_6 that leads to this type of diagonal unit cell (the $\sqrt{2}\sqrt{2}2$-phase must correspond to higher oxygen content than the stoichiometric $TbBaCo_2O_{5.5}$ 122-phase).

The relative phase proportion in samples of $TbBaCo_2O_{6-\delta}$ depends, most likely, on the thermal treatment, in the present case on the velocity of cooling from the synthesis temperature. The NPD studies of the crystal structure of $TbBaCo_2O_{6-\delta}$ and its thermal evolution have been focused on the Q-TBCO and 1C-TBCO samples to minimize difficulties due to the formation of phases with different oxygen content. In this sense and as it is explained in the following sections, the quenched samples lead to 112-phases (type A crystals of Fig. 2), as found in previous results in $GdBaCo_2O_{6-\delta}$ [12] and the 1C-TBCO sample must be near the equilibrium of the oxygen content according to results in $PrBaCo_2O_{6-\delta}$.[25]

3.2. Sample prepared in air and quenched to room temperature (Q-TBCO)

The SAED patterns and HRTEM images of the Q-TBCO sample indicate that the sample is predominantly formed by 112-phase, although some crystals present domains of the 132 phase. The study of the average (long-range) structure has been performed by fitting the XRPD and NPD patterns by the Rietveld method to the structural model given in Table S1. Figure S2 and Figure 5 show the result of the XRPD and NPD data, respectively.
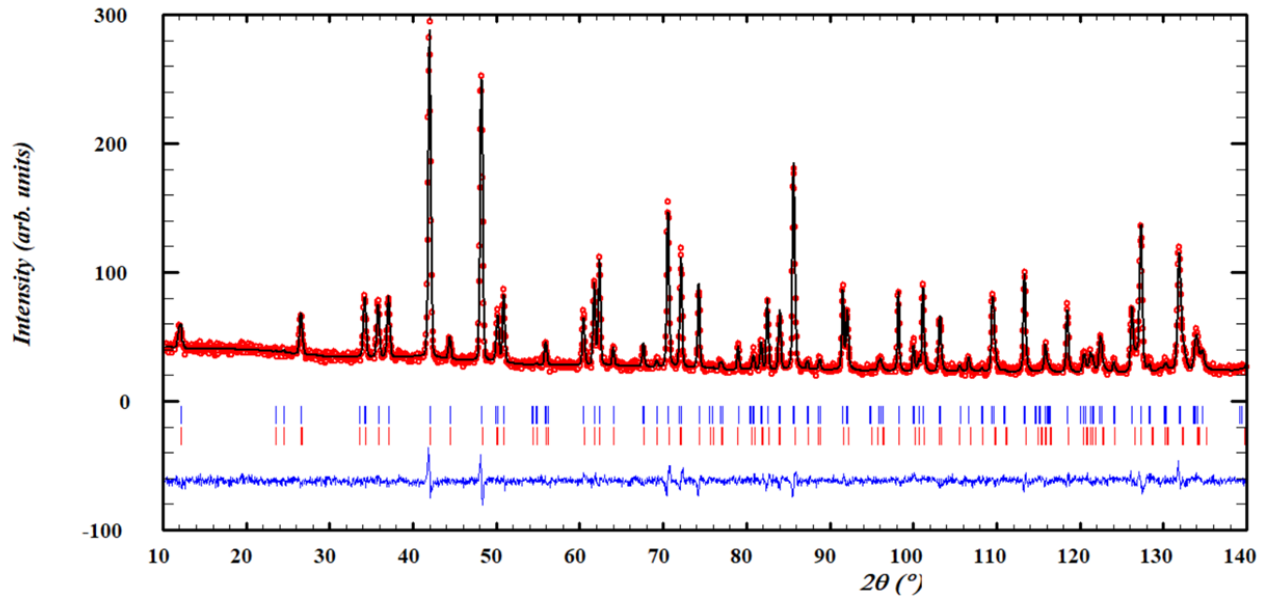
Figure 5. Graphic result of the fitting of the NPD data at room temperature of Q-TBCO. The red points represent the experimental pattern, the continuous black line the calculated using the structural model on Table S1 and the blue line is their difference. Vertical bars indicate the positions of Bragg peaks of the two 112-like phases present.

High-resolution XRPD data reveal the presence two 112-phases (Fig. S2). Besides, the sample seems to contain some amount of the 132-phase, suggested by the presence in the XRPD pattern of the (040) reflection (indicated by an asterisk in Fig. S2). The room temperature NPD data of this Q-TBCO sample confirm the existence of two 112-phases with different oxygen content: 72(4) % (in weight) of the sample consists of a phase with $\delta = 1$ and 28(4) % of a secondary phase corresponding to $\delta = 0.70(1)$. Figures S3a and b show schematic representations of the 112-type crystal structure of the two phases in Q-TBCO. As expected in $TbBaCo_2O_5$, the oxygen deficiency leads to oxygen-empty Tb-planes within the structure and the Co-environment consists of $CoO5$ pyramids. In the phase with higher oxygen content ($\delta = 0.70(1)$) some O3p-oxygen positions within the $TbO1-\delta$ planes are randomly occupied forming $CoO6$ octahedra. Therefore, quenched samples to room temperature led to

112-phases with low oxygen content ($\delta > 0.5$). However, distribution of the oxygen is not homogeneous, but formation of different phases is detected.

3.3. Sample prepared in air and cooled to room temperature at 1 ºC h-1 (1C-TBCO).

Figure S4 shows the result of fitting the XRPD pattern of the 1C-TBCO sample. The pattern can be indexed as a single 122-phase. The SAED and HRTEM results of the 1C-TBCO sample are similar to those of the B-type crystals of the 5C-TBCO sample.

3.3.1 Thermodiffraction of the 1C-TBCO sample

The thermal evolution of the crystal structure of the 122-phase in air was studied by NPD.

Figure 6 presents the graphic result of the fitting of the NPD pattern recorded in air at 200 °C (temperature at which the phase is in its paramagnetic region) with the corresponding structural model given in Table S2.
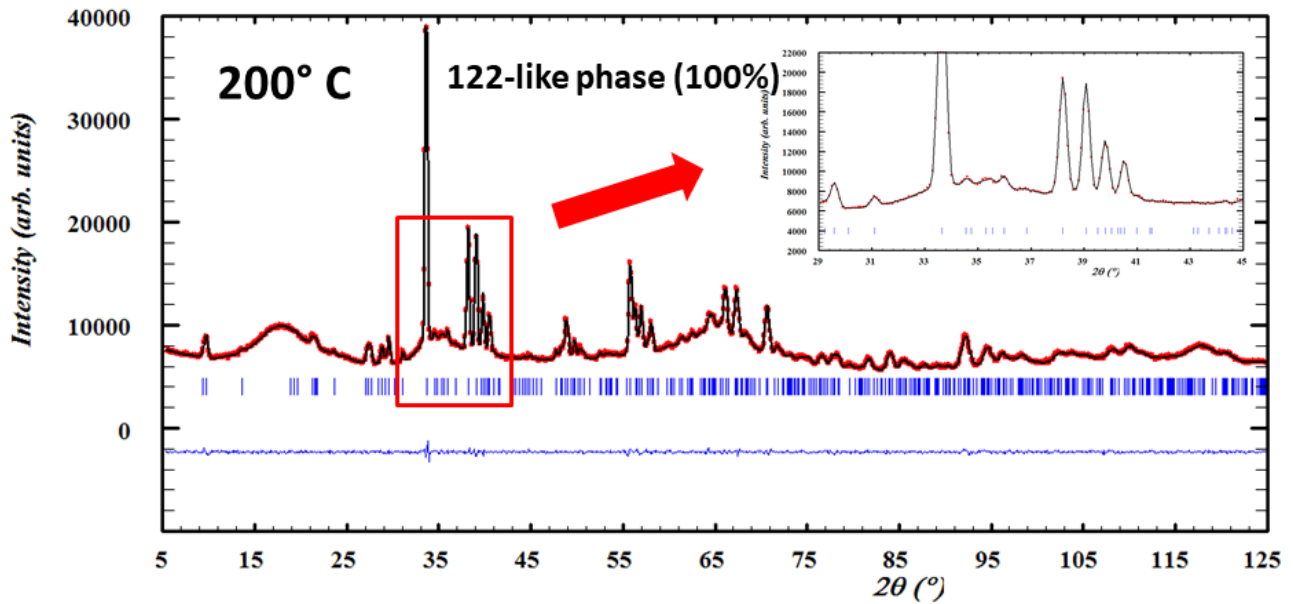
Figure 6. Graphic result of the fitting of the NPD data at 200 °C, on heating in air, of 1C-TBCO sample. The red points represent the experimental pattern, the continuous black line the calculated using the structural model on Table S2 and the blue line is their difference. Vertical bars indicate the positions of Bragg peaks. In the inset shows a zoom of an especially relevant zone of diffraction pattern. The wavy-like background is created by the quartz tube used to assure the contact to air in this furnace experiment.

The pattern can be nicely refined (Table S2) with a single 122-type phase with perfect laminar order of Ba and Tb along the c-axis, and oxygen vacancies ordered along the b-axis within the $TbO_{1-\delta}$ planes, as represented in Figure 7a. According to the cooling procedure in the synthesis of the 1C-TBCO sample and considering that the $LnCo_2O_{5+\delta}$ oxides prepared in air gain oxygen from room temperature to 200 °C,[13,25] the total oxygen content of the 1C-TBCO sample at 200 °C is probably slightly higher than the one corresponding to $\delta = 0.5$. This extra oxygen must be very small, since long time annealing at about 250 °C and relatively high PO_2 are needed to achieve oxygen contents with δ near 0.[25] Besides, since the oxygen distribution seems not be uniform in the particles of the oxide, the extra oxygen could be concentrated in $\sqrt{2}\sqrt{2}2$-nanodomains that cannot be detected from the NPD data.
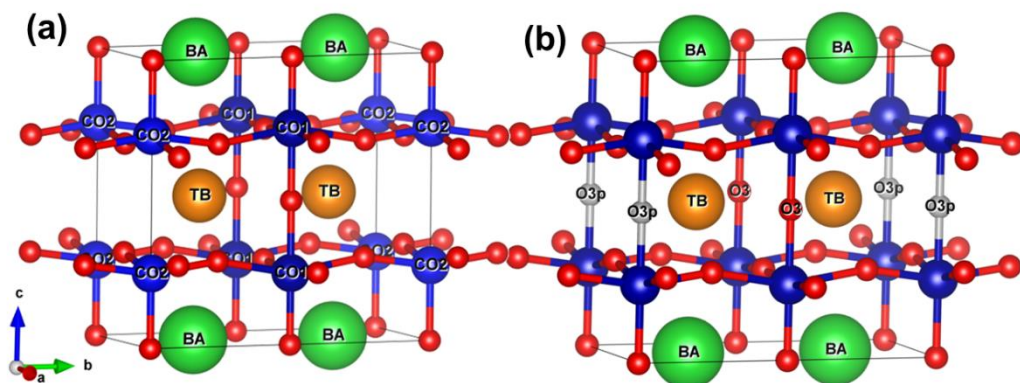
Figure 7. (a) Schematic representation of the structure of ordered 122-like phase: O3 positions are occupied and O3p positions are empty; (b) disordered 122-like structure: both O3 and O3p positions are occupied.

Oxygen release/uptake occurs in these planes (positions O3 and O3p in Table S2) with heating/cooling, whereas the rest of the oxygen sites in the BaO layers (O1 and O2 in Table S2) and CoO_4 layers (O4, O5 and O6 in Table S2) are not labile.

At 300 °C, the NPD results reveals that the oxygen-vacancies in the $TbO_{1-\delta}$ planes begin to disorder; about 5% of the O3p positions in this layer become to be occupied while the occupation of the O3 positions decreases (see Table S2). No relevant oxygen loss is observed.

Further heating to 400 °C induces important changes; the 112-type phase appears together with the disordered 122-phase (Figure 8). In both disordered phases, 122-type and 112-type, oxygen positions within the $TbO_{1-\delta}$ planes are partially occupied (O3 and O3p in Fig. 7) but the oxygen content in the 112-phase is lower (see Table S2)
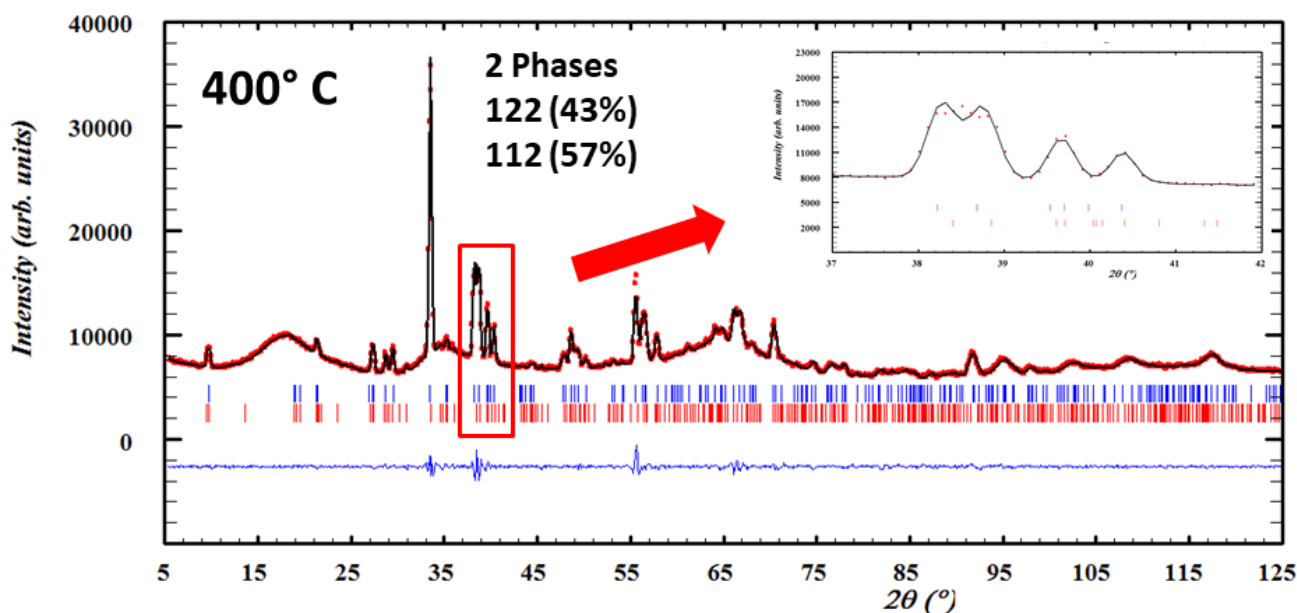

Figure 8. Experimental and calculated NPD patterns at 400 ºC, on heating in air, of 1C-TBCO sample. The red points represent the experimental pattern, the continuous black line the calculated using the structural model on Table S2 and the blue line is their difference. Vertical blue and red bars indicate the positions of nuclear Bragg peaks of the 112 and 122 phases respectively. In the inset shows a zoom of an especially relevant zone of the diffraction pattern.

Thus, the sample at 400 °C consists of a disordered 122-phase (43% in mass) and 57% of a 112-phase with δ >0.5. The oxygen loss starts at this temperature, as common in $LnBaCo_2O_{6-\delta}$ (Ln=Pr, Gd) systems,[13,25] but this oxygen release proceeds with co-existence of different phases.

At 500 °C the 122-phase totally disappears (Figure 9), the sample is single-phase consisting of a disordered tetragonal 112-like phase (Table S2).

Increasing the temperature results in further oxygen loss. At temperatures between 700 and 800 °C most of the oxygen positions in the $TbO_{1-\delta}$ planes of the 112-like phase are

empty, with the remaining small fraction being highly mobile in the layers (Table S2).

By cooling down from 800 °C the sample displays a totally reversible behavior at the cooling rate used in the experiment, which is close to equilibrium conditions (each pattern takes about 4 hours to be collected after 30 min of thermal stabilization). Figures S5 to S7 display the results of the fits of the experimental NPD patterns recorded at 500 °C, 400 °C and 300 °C (when cooling the sample in air from 800 °C), to the models on Table S2. The sample evolution on cooling demonstrates that the oxygen uptake, like the oxygen release, does not occur all over the particles in a homogeneous way but through a mechanism that implies formation of phases with different oxygen contents. The oxygen atoms and vacancies are accommodated within the $TbO_{1-\delta}$ planes during oxygen uptake by modulation from the 112-phase into the 122-phase.

Even at temperatures as high as 800 °C, oxygen atoms are detected within the $TbO_{1-\delta}$ planes (O3p positions) and formation of anion vacancies in other crystallographic positions of the structure does not occur. These results support the high oxygen anisotropy diffusion reported in $PrCo_2O_{6-\delta}$[28] and therefore the essential role of the singular $LnO_{1-\delta}$ layers in the anion conducting properties of $LnCo_2O_{6-\delta}$ layered-type perovskites.[9,10]
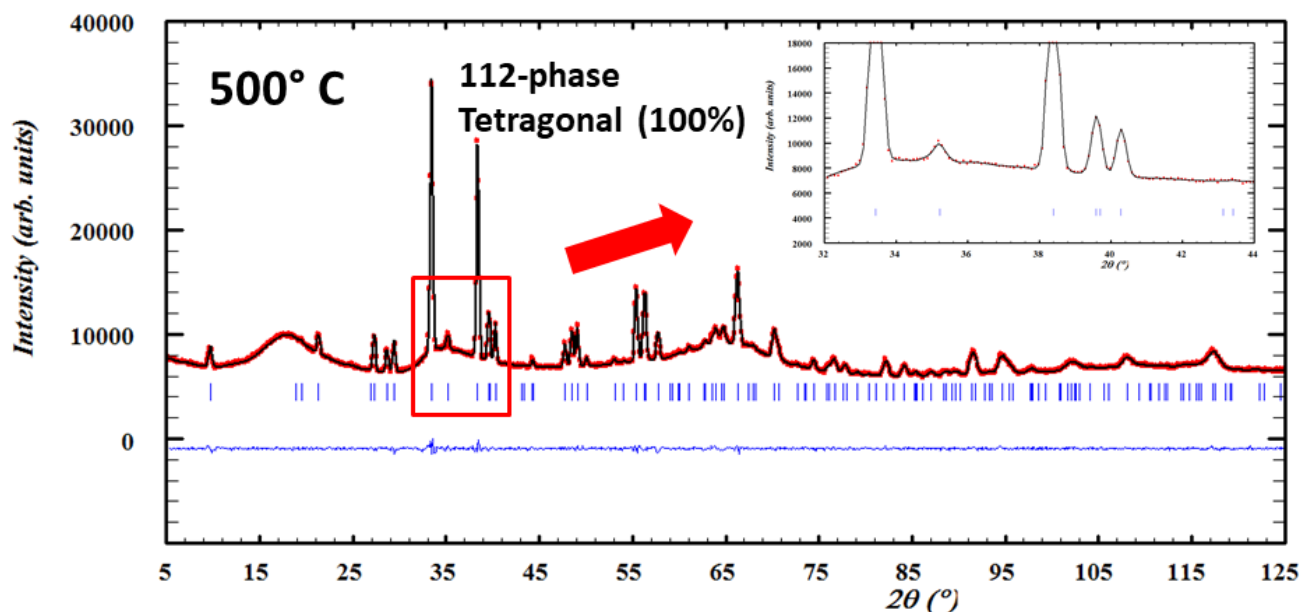

Figure 9. Experimental and calculated NPD patterns at 500 °C, on heating in air, of 1C-TBCO. The red points represent the experimental pattern, the continuous black line the calculated using the structural model on Table S2 and the blue line is their difference. Vertical bars indicate the positions of nuclear Bragg peaks of the 112-phase.

4. CONCLUSIONS

The oxygen content in the $TbBaCo_2O_{6-\delta}$, like previously recognized in $LnBaCo_2O_{6-\delta}$ systems with Ln = Gd, Pr, is dependent on the synthesis conditions and further thermal treatments. Common solid state preparation methods with relatively slow cooling rates lead to coexistence of phases with different oxygen content distributed in nanodomains within the particles. Since the electrical and electrochemical properties of this type of layered perovskites are highly influenced by the anion vacancies concentration and their location in the structure, careful analysis of the formation conditions of stable phases is needed to optimize the properties of these materials for different applications.

The 122 and 112 phases are predominant, indicating that location and ordering of the anion vacancies in the $TbO_{1-\delta}$ planes stabilize the crystal structure. The evolution of the crystal structure of $TbBaCo_2O_{6+\delta}$ during thermal oxygen release on heating consists of modulation from the 122-phase to the 112-phase by creation of anion vacancies within the $TbO_{1-\delta}$ planes. In a similar way, modulation from the 112-phase to the 122-phase takes place during thermal oxygen uptake on cooling by location of oxygens following an ordered pattern. Location of the anion vacancies within the $TbO_{1-\delta}$ planes even at the highest temperatures of the study support the 2D character of the high anion conduction of the $LnBaCo_2O_{6-\delta}$ oxides.

ASSOCIATED CONTENT

(Word Style "TE_Supporting_Information"). **Supporting Information**. A brief statement in nonsentence format listing the contents of material supplied as Supporting Information should be included, ending with "This material is available free of charge via the Internet at http://pubs.acs.org." For instructions on what should be included in the Supporting Information as well as how to prepare this material for publication, refer to the journal's Instructions for Authors.

AUTHOR INFORMATION

Corresponding Author

Susana García-Martín - Departamento de Química Inorgánica I, Facultad de Ciencias Químicas, Universidad Complutense,

28040 Madrid, Spain

Email: sgmartin@quim.ucm.es

Authors

Ulises Amador – Departamento de Química y Bioquímica, Facultad de Farmacia, Universidad CEU San Pablo, E-28668 Madrid, Spain; orcid.org/0000-0002-4412-2419

Rafael Marín- Departamento de Química Inorgánica I, Facultad de Ciencias Químicas, Universidad Complutense, 28040 Madrid, Spain

Clemens Ritter – Institut Laue-Langevin, BP 156-38042, Grenoble, Cedex 9, France; orcid.org/0000-0003-3674-3378

Oscar Fabelo – Institut Laue-Langevin, BP 156-38042 Grenoble, Cedex 9, France; orcid.org/0000-0001-6452-8830

M. Teresa Azcondo – Departamento de Química y Bioquímica, Facultad de Farmacia, Universidad CEU San Pablo, E-28668, Madrid, Spain; orcid.org/0000-0002-3890-0800

Author Contributions

All authors contributed equally.

Funding Sources

Any funds used to support the research of the manuscript should be placed here (per journal style).

Notes

Any additional relevant notes should be placed here.

ACKNOWLEDGMENT

REFERENCES

(1) Kilner, J. A.; Burriel, M. Materials for Intermediate-Temperature Solid-Oxide Fuel Cells. *Annu. Rev. Mater. Res.* **2014**, *44*, 365–393. https://doi.org/10.1146/annurev-matsci-070813-113426.

(2) Kim, J. H.; Manthiram, A. Layered LnBaCo2O5+δ Perovskite Cathodes for Solid Oxide Fuel Cells: An Overview and Perspective. *J. Mater. Chem. A* **2015**, *3* (48), 24195–24210. https://doi.org/10.1039/c5ta06212h.

(3) Pelosato, R.; Cordaro, G.; Stucchi, D.; Cristiani, C.; Dotelli, G. Cobalt Based Layered Perovskites as Cathode Material for Intermediate Temperature Solid Oxide Fuel Cells: A Brief Review. *J. Power Sources* **2015**, *298*, 46–67. https://doi.org/https://doi.org/10.1016/j.jpowsour.2015.08.034.

(4) Gao, Z.; Mogni, L. V; Miller, E. C.; Railsback, J. G.; Barnett, S. A. A Perspective on Low-Temperature Solid Oxide Fuel Cells. *Energy Environ. Sci.* **2016**, *9* (5), 1602–1644. https://doi.org/10.1039/C5EE03858H.

(5) Guan, D.; Zhou, J.; Huang, Y.-C.; Dong, C.-L.; Wang, J.-Q.; Zhou, W.; Shao, Z. Screening Highly Active Perovskites for Hydrogen-Evolving Reaction via Unifying Ionic Electronegativity Descriptor. *Nat. Commun.* **2019**, *10* (1), 3755. https://doi.org/10.1038/s41467-019-11847-w.

(6) Guan, D.; Zhou, J.; Hu, Z.; Zhou, W.; Xu, X.; Zhong, Y.; Liu, B.; Chen, Y.; Xu, M.; Lin, H.-J.; et al. Searching General Sufficient-and-Necessary Conditions for Ultrafast Hydrogen-Evolving Electrocatalysis. *Adv. Funct. Mater.* **2019**, *29* (20), 1900704. https://doi.org/https://doi.org/10.1002/adfm.201900704.

(7) Sun, Q.; Dai, Z.; Zhang, Z.; Chen, Z.; Lin, H.; Gao, Y.; Chen, D. Double Perovskite PrBaCo2O5.5: An Efficient and Stable Electrocatalyst for Hydrogen Evolution Reaction. *J. Power Sources* **2019**, *427*, 194–200.

(8) Marelli, E.; Gazquez, J.; Poghosyan, E.; Müller, E.; Gawryluk, D. J.; Pomjakushina, E.; Sheptyakov, D.; Piamonteze, C.; Aegerter, D.; Schmidt, T. J.; et al. Correlation between Oxygen Vacancies and Oxygen Evolution Reaction Activity for a Model Electrode: PrBaCo2O5+δ. *Angew. Chemie Int. Ed.* **2021**, *60* (26), 14609–14619. https://doi.org/https://doi.org/10.1002/anie.202103151.

(9) Taskin, A. A.; Lavrov, A. N.; Ando, Y. Fast Oxygen Diffusion in A-Site Ordered Perovskites. *Prog. Solid State Chem.* **2007**, *35* (2), 481–490. https://doi.org/https://doi.org/10.1016/j.progsolidstchem.2007.01.014.

(10) Parfitt, D.; Chroneos, A.; Tarancón, A.; Kilner, J. A. Oxygen Ion Diffusion in Cation Ordered/Disordered GdBaCo2O 5+δ. *J. Mater. Chem.* **2011**, *21* (7), 2183–2186. https://doi.org/10.1039/c0jm02924f.

(11) Chang, A.; Skinner, S. J.; Kilner, J. A. Electrical Properties of GdBaCo2O5+x for ITSOFC Applications. *Solid State Ionics* **2006**, *177* (19-25 SPEC. ISS.), 2009–2011. https://doi.org/10.1016/j.ssi.2006.05.047.

(12) Tarancón, A.; Skinner, S. J.; Chater, R. J.; Hernández-Ramírez, F.; Kilner, J. A. Layered Perovskites as Promising Cathodes for Intermediate Temperature Solid Oxide Fuel Cells. *J. Mater. Chem.* **2007**, *17* (30), 3175–3181. https://doi.org/10.1039/b704320a.

(13) Muñoz-Gil, D.; Pérez-Coll, D.; Peña-Martínez, J.; Garcia-Martín, S. New Insights into the GdBaCo2O5+δ Material: Crystal Structure, Electrical and Electrochemical Properties. *J. Power Sources* **2014**, *263*, 90–97. https://doi.org/https://doi.org/10.1016/j.jpowsour.2014.04.019.

(14) Maignan, A.; Martin, C.; Pelloquin, D.; Nguyen, N.; Raveau, B. Structural and Magnetic Studies of Ordered Oxygen-Deficient PerovskitesLnBaCo2O5+δ, Closely Related to the "112" Structure. *J. Solid State Chem.* **1999**, *142* (2), 247–260. https://doi.org/https://doi.org/10.1006/jssc.1998.7934.

(15) Kim, W. S.; Chi, E. O.; Choi, H. S.; Hur, N. H.; Oh, S.-J.; Ri, H.-C. Reentrant Paramagnetic Behavior and Spin-State Transition in the Layered Cobalt Oxide GdBaCo2O5+δ. *Solid State Commun.* **2000**, *116* (11), 609–614. https://doi.org/https://doi.org/10.1016/S0038-1098(00)00385-9.

(16) Moritomo, Y.; Akimoto, T.; Takeo, M.; Machida, A.; Nishibori, E.; Takata, M.; Sakata, M.; Ohoyama, K.; Nakamura, A. Metal-Insulator Transition Induced by a Spin-State Transition in ${\mathrm{TbBaCo}}_{2}{\mathrm{O}}_{5+\ensuremath{\delta}} (\ensuremath{\delta}=0.5)$. *Phys. Rev. B* **2000**, *61* (20), R13325–R13328. https://doi.org/10.1103/PhysRevB.61.R13325.

(17) Frontera, C.; Garc\'\ia-Muñoz, J. L.; Llobet, A.; Aranda, M. A. G. Selective Spin-State Switch and Metal-Insulator Transition in GdBaCo2O5+δ. *Phys. Rev. B* **2002**, *65* (18), 180405. https://doi.org/10.1103/PhysRevB.65.180405.

(18) Taskin, A. A.; Lavrov, A. N.; Ando, Y. Transport and Magnetic Properties of GdBaCo2O5+x Single Crystals: A Cobalt Oxide with Square-Lattice CoO2 Planes over a Wide Range of Electron and Hole Doping. *Phys. Rev. B* **2005**, *71* (13), 134414. https://doi.org/10.1103/PhysRevB.71.134414.

(19) Anderson, P. S.; Kirk, C. A.; Knudsen, J.; Reaney, I. M.; West, A. R. Structural Characterisation of REBaCo2O6−δ Phases (RE=Pr, Nd, Sm, Eu, Gd, Tb, Dy, Ho). *Solid State Sci.* **2005**, *7* (10), 1149–1156. https://doi.org/https://doi.org/10.1016/j.solidstatesciences.2005.03.004.

(20) Tarancón, A.; Marrero-López, D.; Peña-Martínez, J.; Ruiz-Morales, J. C.; Núñez, P. Effect of Phase Transition on High-Temperature Electrical Properties of GdBaCo2O5+x Layered Perovskite. *Solid State Ionics* **2008**, *179* (17), 611–618. https://doi.org/10.1016/j.ssi.2008.04.028.

(21) Mogni, L.; Prado, F.; Jiménez, C.; Caneiro, A. Oxygen Order–Disorder Phase Transition in Layered GdBaCo2O5+δ Perovskite: Thermodynamic and Transport Properties. *Solid*

State Ionics **2013**, *240*, 19–28. https://doi.org/https://doi.org/10.1016/j.ssi.2013.03.021.

(22) Ishizawa, N.; Asaka, T.; Kudo, T.; Fukuda, K.; Abe, N.; Arima, T. Incommensurate Structure of GdBaCo2O5+δ (Δ∼0.38). *J. Solid State Chem.* **2013**, *198*, 532–541. https://doi.org/https://doi.org/10.1016/j.jssc.2012.11.004.

(23) Zhou, L.; Han, Y.; Yin, C.; Wang, Y.; Yang, X.; Allix, M.; Huang, Q.; Xiong, J.; Wang, B.; Li, G.; et al. Trigonal-Planar Low-Spin Co2+ in a Layered Mixed-Polyhedral Network from Topotactic Reduction. *Inorg. Chem.* **2019**, *58* (20), 14193–14203. https://doi.org/10.1021/acs.inorgchem.9b02244.

(24) Karen, P. Thermal Evolution of the EuBaCo2O5.5 Crystal Structure. *J. Solid State Chem.* **2022**, *311*, 123102. https://doi.org/https://doi.org/10.1016/j.jssc.2022.123102.

(25) Frontera, C.; Caneiro, A.; Carrillo, A. E.; Oró-Solé, J.; García-Muñoz, J. L. Tailoring Oxygen Content on PrBaCo2O5+δ Layered Cobaltites. *Chem. Mater.* **2005**, *17* (22), 5439–5445. https://doi.org/10.1021/cm051148q.

(26) Rodríguez-Carvajal, J. Recent Advances in Magnetic Structure Determination by Neutron Powder Diffraction. *Phys. B Condens. Matter* **1993**, *192* (1), 55–69. https://doi.org/https://doi.org/10.1016/0921-4526(93)90108-I.

(27) Le Bail, A.; Duroy, H.; Fourquet, J. L. Ab-Initio Structure Determination of LiSbWO6 by X-Ray Powder Diffraction. *Mater. Res. Bull.* **1988**, *23* (3), 447–452. https://doi.org/https://doi.org/10.1016/0025-5408(88)90019-0.

(28) Burriel, M.; Peña-Martínez, J.; Chater, R. J.; Fearn, S.; Berenov, A. V; Skinner, S. J.; Kilner, J. A. Anisotropic Oxygen Ion Diffusion in Layered PrBaCo2O5+δ. *Chem. Mater.* **2012**, *24* (3), 613–621. https://doi.org/10.1021/cm203502s.

$TbBaCo_2O_{6-\delta}$, with layered perovskite-type structure, accommodates the oxygen vacancies in different ordering patterns. Different phases are obtained through oxygen release/uptake by heating/cooling in air, which occurs within the $TbO_{1-\delta}$ planes. At the temperatures the material works as cathode in solid oxide fuel cells, the structure is tetragonal and a noticeably concentration of interstitial oxygen remains in those planes, explaining the 2D character of its high ionic conduction and its good electrochemical performance.